crystals

MDPI

Article

High-Pressure Reactivity of Kr and F_2—Stabilization of Krypton in the +4 Oxidation State

Dominik Kurzydłowski [1,2,*], Magdalena Sołtysiak [2], Aleksandra Dżoleva [2] and Patryk Zaleski-Ejgierd [3,*]

1 Centre of New Technologies, University of Warsaw, 02-097 Warsaw, Poland
2 Faculty of Mathematics and Natural Sciences, Cardinal Stefan Wyszyński University, 01-038 Warsaw, Poland; magdalena.soltysiak.uksw@gmail.com (M.S.); aleksandradzoleva@poczta.onet.pl (A.D.)
3 Faculty of Physics, IFT, University of Warsaw, 02-093 Warsaw, Poland
* Correspondence: d.kurzydlowski@cent.uw.edu.pl (D.K.); pzaleski@fuw.edu.pl (P.Z-E.)

Academic Editor: Ralf Haiges
Received: 29 September 2017; Accepted: 25 October 2017; Published: 28 October 2017

Abstract: Since the synthesis of the first krypton compound, several other Kr-bearing connections have been obtained. However, in all of them krypton adopts the +2 oxidation state, in contrast to xenon which forms numerous compounds with an oxidation state as high as +8. Motivated by the possibility of thermodynamic stabilization of exotic compounds with the use of high pressure (exceeding 1 GPa = 10 kbar), we present here theoretical investigations into the chemistry of krypton and fluorine at such large compression. In particular we focus on krypton tetrafluoride, KrF_4, a molecular crystal in which krypton forms short covalent bonds with neighboring fluorine atoms thus adopting the +4 oxidation state. We find that this hitherto unknown compound can be stabilized at pressures below 50 GPa. Our results indicate also that, at larger compressions, a multitude of other Kr_mF_n fluorides should be stable, among them KrF which exhibits covalent Kr–Kr bonds. Our results set the stage for future high-pressure synthesis of novel krypton compounds.

Keywords: krypton; fluorine; high-pressure; Density Functional Theory; phase transitions; noble-gas chemistry; molecular crystals, fluorides

1. Introduction

Among the non-radioactive group 18 elements (He, Ne, Ar, Kr, Xe) only the two heaviest, krypton and xenon, form compounds isolable in macroscopic quantities. With its lowest first ionization potential (12.13 eV) xenon forms numerous compounds in which it adopts oxidation states +1/2, +2, +4, +6 and +8 [1–6]. The relatively large thermodynamic and/or kinetic stability of these species enabled characterization of over 150 crystal structures for Xe-bearing systems.

Due to its higher ionization potential (14.0 eV), krypton is much less reactive and forms compounds only in the +2 oxidation state [7–9]. All of these connections are derived from krypton difluoride (KrF_2), a compound discovered in 1963 [10–13], only a year after Bartlett's landmark synthesis of the first xenon compound [14,15]. In contrast to xenon difluoride (XeF_2), KrF_2 is thermodynamically unstable (ΔH_f = 60.2 kJ mol^{-1}, at 93 °C [16]) and thus hard to synthesize and handle. Higher fluorides of krypton (KrF_4, KrF_6) are not known (initial reports of the synthesis of KrF_4 [10,11] have never been confirmed), again in contrast to xenon which does form both XeF_4 and XeF_6. Despite the mediocre reactivity of krypton a substantial number of compounds and complexes containing this element were speculated to exist in the gas phase [17–23].

The next group 18 element, argon, exhibits an even higher first ionization potential (15.8 eV), and consequently forms transient species which can be stabilized only in low-temperature matrices or in the gas-phase [24–29]. The decreased reactivity of argon is also manifested by the fact that at ambient

pressure it does not form any fluoride, even at low temperature. However, our recent computational investigation indicated that argon difluoride (ArF_2) can be thermodynamically stabilized (i.e., possess a negative enthalpy of formation) at pressures above 60 GPa (=600 kbar) [30].

While 60 GPa may seem high on the pressure scale, such conditions are now routinely achieved in experiments conducted with the use of diamond anvil cells (DACs). In recent years, there is a growing interest in the high-pressure chemistry of noble gases concerning both experiment [31–35], and theory [36–40]. In particular, much attention has been paid to the high-pressure phase transformations of XeF_2 [41–44]. At ambient pressure this compound forms a molecular crystal composed of weakly interacting XeF_2 molecules (in the form of linear and symmetric F–Xe–F units). Early high-pressure investigations indicated that above 50 GPa XeF_2 adopts a graphite-like hexagonal structure, and upon further compression to 70 GPa transforms to a metallic three-dimensional fluorite-like structure [41]. These findings were put into doubt by theory [42], and subsequent experiments indicated that XeF_2 remains molecular and insulating up to 80 GPa [43]. Furthermore, a recent theoretical investigation on the high-pressure thermodynamic stability of Xe_mF_n phases indicated that XeF_2 should decompose into XeF_4 and Xe_2F above 81 GPa [44]. Interestingly Xe_2F, which is not known at ambient conditions, was predicted to exhibit direct Xe–Xe bonds [44].

Noble-gas compounds are text-book examples of systems exhibiting hypervalency, multi-center and charge-shift bonding [45]. Motivated by the peculiar chemistry of Xe/F mixtures at large compression, we performed a systematic theoretical study on the high-pressure thermodynamic stability of various Kr_mF_n crystalline compounds. Our aim was to verify whether novel krypton fluorides might be stabilized at large compression. Employing the Density Functional Theory (DFT) we analyzed 11 possible stoichiometries including both species that are krypton rich (Kr_6F, Kr_4F, Kr_3F, Kr_2F, Kr_3F_2), fluorine rich (Kr_2F_3, KrF_2, KrF_3, KrF_4, KrF_6), as well as KrF. Our study models the 0–200 GPa pressure range which is accessible to modern experiments.

We found that novel connections between krypton and fluorine should indeed stabilize at large compression. In particular, our results indicate that fluorine should oxidize krypton difluoride at high pressure to yield KrF_4—a first example of a compound containing krypton in the +4 oxidation state. We also predict formation of KrF at 100 GPa, which is a compound containing direct Kr–Kr bonds. By comparing our results with previous investigations, we propose general trends in the high-pressure reactivity of noble-gas difluorides.

2. Results

For each of the studied Kr_mF_n compounds we propose crystal structures and perform geometry optimization at high pressure utilizing the DFT method in its periodic approach. We also optimize the structures of solid Kr and F_2. Due to the large complexity of solid-state structures, proposing good high-pressure candidate crystal structures is challenging. In recent years, considerable effort was put into developing algorithms which enable effective structure search for a solid compound of given composition [46–49]. In this study, we performed crystal structure searches employing the USPEX (Universal Structure Predictor: Evolutionary Xtallography) evolutionary algorithm [50,51]—in all of them the only input information was the stoichiometry of the compound and the pressure at which the search was conducted (for more computational details see Materials and Methods).

Our calculations do not include temperature effects, and thus give the thermodynamic stability at the 0 K temperature limit. Due to the large computational burden associated with calculating vibrational properties of solids, neglecting finite-temperature corrections is a standard approach in high-pressure computational chemistry. At the T = 0 K limit, the Gibbs free energy (G) can be equated to the enthalpy (H), and hence at a given pressure the thermodynamic stability of a compound will be governed by its enthalpy.

In this work we define the enthalpy of formation, $\Delta H_f(Kr_mF_n)$ at a given pressure as:

$$\Delta H_f(Kr_mF_n) = [H(Kr_mF_n) - m \cdot H(Kr) - n/2 \cdot H(F_2)]/(m + n), \quad (1)$$

where $H(Kr_mF_n)$, $H(Kr)$, and $H(F_2)$ are the calculated enthalpies of Kr_mF_n, Kr, and F_2 at each pressure. Equation (1) gives $\Delta H_f(Kr_mF_n)$ values per atom, and ensures that $\Delta H_f(Kr) = \Delta H_f(F_2) = 0$. In order to assess the relative thermodynamic stability of various Kr_mF_n phases, as well as their decomposition into Kr and F_2, we use the enthalpies of formation defined above to construct the so-called tie-line plot [52]. In this representation, $\Delta H_f(Kr_mF_n)$ values are plotted against the mole fraction of F atoms. It can be shown that a phase is thermodynamically stable if no tie-line passes below it [52].

2.1. Pressures Up to 50 GPa

We start our discussion with the results obtained in the pressure regime up to 50 GPa. We find that the thermodynamic stability of various phases differs qualitatively in this pressure range compared to results obtained at higher compression (see Section 2.2). In Figure 1a we display a tie-line plot of the Kr/F system for pressures of 0 GPa (1 bar = 10^{-4} GPa; ambient pressure thus equals effectively to 0 GPa), 15 GPa and 50 GPa.

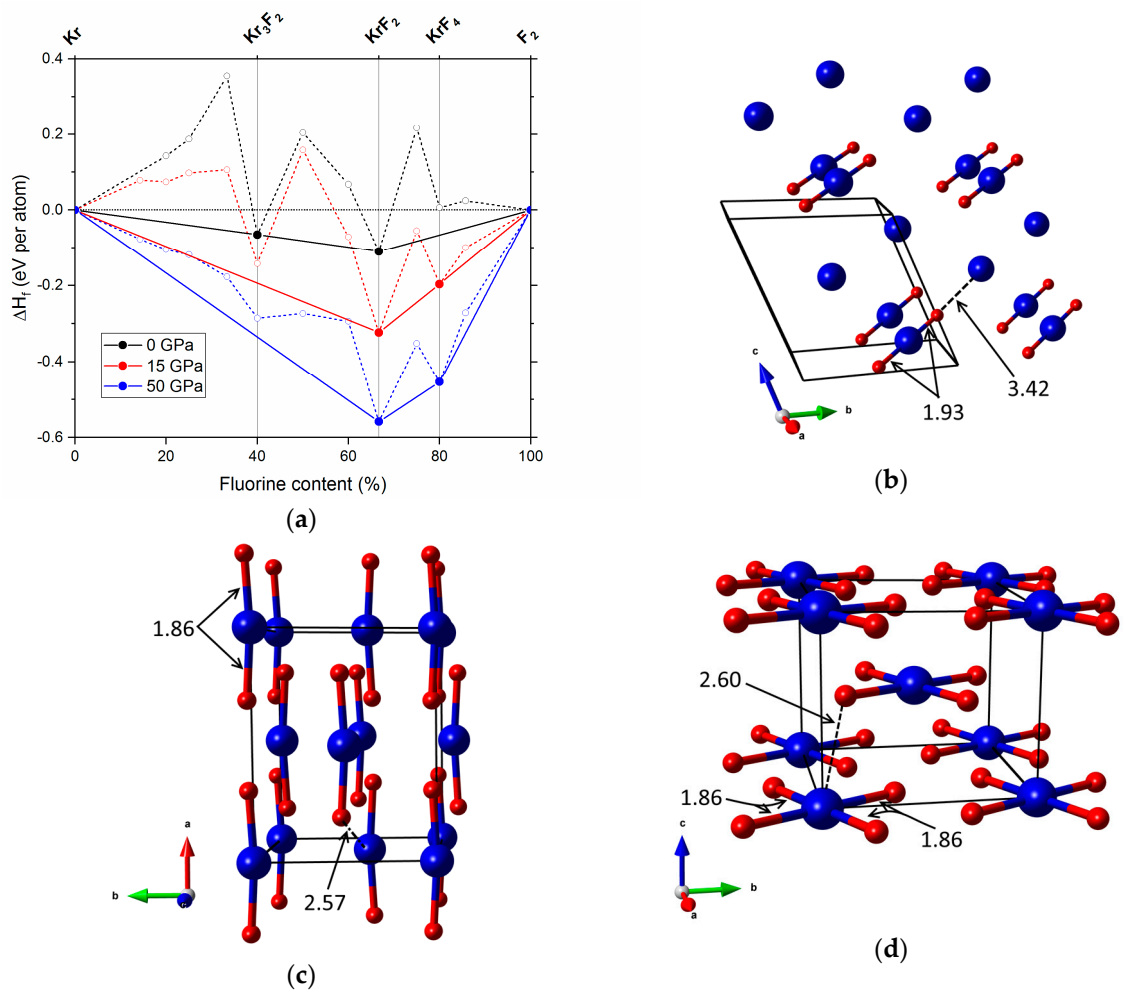

Figure 1. (**a**) Pressure dependence of the enthalpy of formation per atom of various Kr_mF_n phases at 0, 15 and 50 GPa. The compounds stable at 0 GPa (Kr_3F_2, KrF_3), 15 GPa (KrF_2, KrF_4) and 50 GPa (KrF_2, KrF_4) are marked in the upper part of the graph; (**b**) The *P1* structure of Kr_3F_2 (=2Kr·KrF_2) at 0 GPa; (**c**) The *Cmcm* structure of KrF_2 at 50 GPa; (**d**) the *I4/m* structure of KrF_4 at 50 GPa; blue/red balls depict Kr/F atoms; Kr–F bonds (solid lines) and shortest intermolecular Kr–F contacts (dashed lines) are given in Å.

At ambient pressure two compositions are located on the convex hull (i.e., there are no tie-lines passing below them, and hence they are thermodynamically stable). These are Kr_3F_2 and KrF_2. Inspection of the structure of the former compound (Figure 1b), indicates that it is composed of linear F–Kr–F molecules, characterized by a Kr–F bond length of 1.93 Å, and unbound Kr atoms (nearest Kr–F contact at 3.42 Å). Therefore, a more realistic formulation of Kr_3F_2 would be $2Kr{\cdot}KrF_2$—that is a co-crystal of Kr and KrF_2. This phase quickly destabilizes at high pressures, and is predicted to decompose into Kr and KrF_2 already at 1 GPa.

The other stable compound at ambient conditions is KrF_2. At 0 GPa, our evolutionary searches identify two structures of *I4/mmm* and *P4$_2$/mnm* symmetry which are nearly degenerate in terms of enthalpy. These correspond respectively to the experimentally known ambient-pressure α and β polymorphs of KrF_2 [53,54]. Both of them contain linear F–Kr–F units with a Kr–F bond length of 1.93 Å. Application of pressures up to 6 GPa leads to thermodynamic stabilization of the *I4/mmm* structure over *P4$_2$/mnm*. Above 6 GPa we predict a phase transition from *I4/mmm* to a structure of *Cmcm* symmetry composed of slightly bent F–Kr–F molecules (173° at 50 GPa, see Figure 1c). This polymorph of KrF_2, which is isostructural to the predicted high-pressure phase of ArF_2 [30], remains the most stable structure up to 200 GPa. Even at that pressure it retains its molecular character with Kr–F bonds (1.78 Å) still much shorter than the Kr–F intermolecular contacts (2.19 Å).

We predict that at 0 GPa KrF_2 is marginally stable with respect to decomposition into Kr and F_2 ($\Delta H_f = -0.08$ eV/atom). In contrast, the experimental enthalpy of formation at ambient pressure is slightly positive (0.21 eV/atom [16]). This value was well reproduced with rigorous coupled-cluster calculations of Dixon et al. [55]. In our previous study, we found that the Perdew–Burke–Ernzerhof (PBE) functional used here tends to overestimate the thermodynamic stability of noble-gas compounds, and that more accurate values can be generally achieved with the application of the hybrid HSE06 functional [30]. Indeed, calculation performed with the use of this functional gives $\Delta H_f(KrF_2) = 0.06$ eV/atom, much closer to the theoretical value of Dixon et al. (0.21 eV/atom, [55]). However, the high computational cost of the HSE06 functional severely restricts the number of compounds that can be studied. Therefore, here we opted to work with the less accurate PBE functional, which however enabled us to screen a much larger array of possible stoichiometries. We emphasize that the pressure dependence of ΔH_f is the same at both the PBE and HSE06 level of theory (see Figure S2 in the Supplementary Material, SM). This gives us confidence that the thermodynamic stabilization of krypton fluorides that we observe at high pressure is not a computational artifact, although the pressure at which a given compound becomes stable might be underestimated (vide infra the case of KrF_4).

The first novel krypton fluoride that becomes thermodynamically stable at elevated pressure is KrF_4; it becomes part of the convex hull already at 15 GPa (Figure 1a). This indicates that KrF_4 should be accessible at high pressures through a reaction of KrF_2 with F_2 or by reacting Kr and F_2 in a 1:2 or greater ratio. Considering the abovementioned over-binding of Kr_mF_n compounds at the applied level of theory (DFT/PBE) the experimental pressure of synthesis might be higher by about 25 GPa, i.e., reach 40 GPa. Indeed, HSE06 calculations indicate that KrF_4 should be stable above that pressure (Figure S2 in SM). We note that such pressure is still in the range of modern experimental techniques.

The most stable structure of KrF_4 in the entire considered pressure range—up to 200 GPa—is a molecular crystal of *I4/m* symmetry composed of weakly interacting square-planar KrF_4 units (Figure 1d). Even at 200 GPa, the Kr–F bond within these molecules (1.77 Å) is more than 20% shorter than the closest Kr–F intermolecular contact (2.26 Å). In fact, the crystal structure of KrF_4 is analogous to the predicted high-pressure phase of XeF_4, which is also molecular even at large compression [44].

To confirm the presence of four covalent Kr–F bonds in KrF_4, we perform an analysis of the Electron Localization Function (ELF) [56]. This dimensionless function, defined for every point in the crystal structure, spans values from 0 to 1. Values close to 1 are generally interpreted as indicating paired electrons (i.e., lone pairs, bonds, and core electrons). Typical covalent bonds are characterized by ELF values of exceeding 0.7; however, previous studies indicated that the maximum ELF value

for the Xe–F bond in XeF_2 is only 0.5 [42,44]. This can be rationalized by taking into account that this bond arises from a three-center two-electron interaction, and is characterized by a bond order of 1/2. By analogy, the same applies to the Kr–F bond in KrF_2, for which we obtain a maximum ELF value of 0.4 (Figure 2a). This is slightly lower than the value found for XeF_2 in accordance with the fact that Kr–F is a weaker bond. More importantly, we find the same ELF values of 0.4 for Kr–F bonds in the KrF_4 molecules present in the *I4/m* structure (Figure 2b), which indicates that in this particular phase krypton forms four *covalent* connections to fluorine atoms; therefore, it can be assigned an oxidation state of +4.

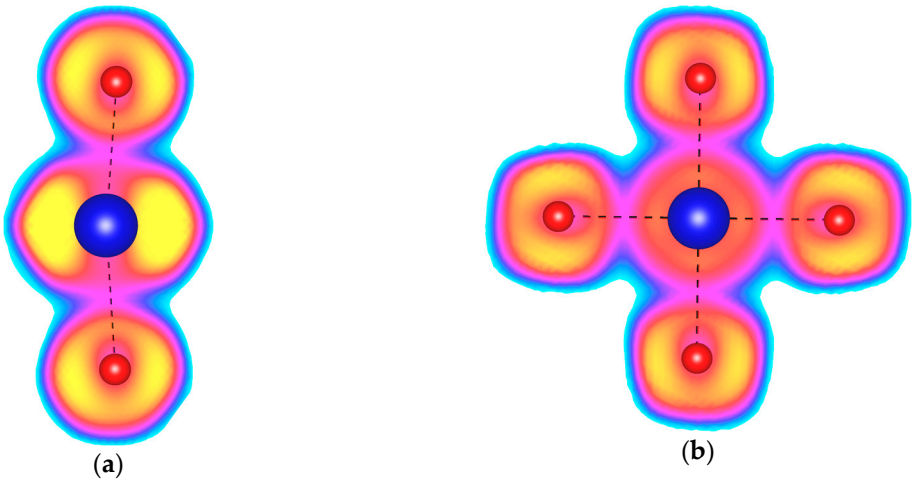

Figure 2. The Electron Localization Function (ELF) plotted for (**a**) the KrF_2 molecules found in the *Cmcm* phase of KrF_2 at 150 GPa; (**b**) the KrF_4 molecules found in the *I4/m* phase of KrF_4 at 150 GPa. Yellow color depicts ELF values above 0.9, cyan—below 0.1, while magenta corresponds to values of 0.4. Kr–F covalent bonds are depicted with a black dashed line.

2.2. The 50–200 GPa Pressure Range

Our calculations indicate that KrF_4 remains thermodynamically stable up to the highest pressure considered in this study (200 GPa). We also do not find any pressure range at which KrF_6—the only Kr_mF_n compound with greater fluorine content than KrF_4—would exhibit thermodynamic stability. However, we do find that some less-fluorine rich Kr_mF_n phases stabilize at pressures larger than 50 GPa. In particular, on the krypton-rich side of the phase diagram we find Kr_6F and Kr_4F becoming part of the convex hull at approx. 80 GPa (Figure 3), and remaining thermodynamically stable up to 200 GPa. Therefore, one should expect formation of these compounds in krypton-rich Kr/F mixtures upon compression.

At higher pressures we predict stabilization of KrF (at 100 GPa), and Kr_2F (at 140 GPa). Both of them remain on the convex hull up to 200 GPa. Interestingly, we find that KrF_2 becomes thermodynamically unstable above 180 GPa—above that pressure it should spontaneously decompose into the hitherto unknown KrF and KrF_4.

Within their pressure stability range, Kr_6F and Kr_4F do not exhibit any phase transitions. The lowest-enthalpy structures of these krypton-rich phases are formed by closely packed Kr atoms decorated with isolated F atoms (see Figure S3 in the SM). As shown in Table 1, the Kr–F distances found in these compounds are considerably longer than the covalent Kr–F bonds in KrF_2 and KrF_4. On the other hand, Kr–Kr contacts are comparable to those found in solid Kr at the same pressure. These characteristic features indicate that the building blocks of both Kr_6F and Kr_4F consist of atoms rather than molecules, and that these compounds lack covalent bonding. The latter point is confirmed by the analysis of the ELF function for these compounds, which indicates that ELF values calculated

between all of the atoms do not exceed 0.1. This number is comparable to the value found between Kr atoms in solid krypton at the same pressure (Figure S4 in SM).

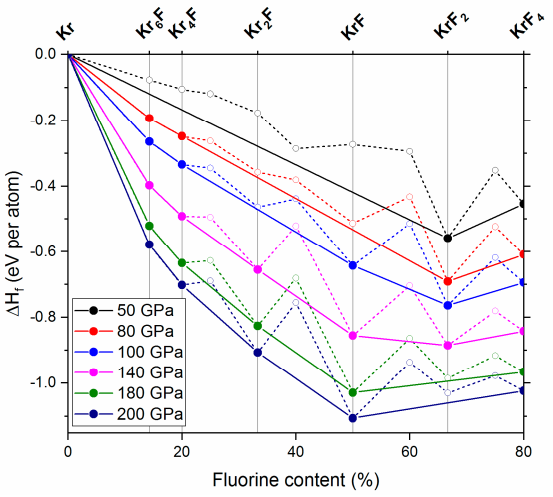

Figure 3. Pressure dependence of the enthalpy of formation per atom of various Kr_mF_n phases at 50, 80, 100, 140, 180 and 200 GPa. The compounds which stabilize at 80 GPa (Kr_6F, Kr_4F), 100 GPa (KrF) and 140 GPa (Kr_2F) are marked together with KrF_2 and KrF_4 in the upper part of the graph; note that KrF_2 is predicted to decompose above 180 GPa.

Table 1. Comparison of the closest Kr–F, Kr–Kr and F–F distances (in Å) for the lowest enthalpy structures of Kr_mF_n compounds at 150 GPa.

Phase	Type	Kr–F	Kr–Kr	F–F
Kr	Atomic (3D)	-	2.68–2.75	-
Kr_6F		2.29–2.39	2.58–2.77	2.78
Kr_4F		2.31–2.34	2.62–2.70	2.68
Kr_2F	2D	2.29	2.51–2.56; 2.83–2.84	2.21
KrF	1D	2.27–2.33	2.29; 2.78–2.90	2.29
KrF_2	Molecular (0D)	1.80	2.66	2.19
KrF_4		1.80	3.57	2.00
F_2		-	-	1.42

For Kr_2F, our structure investigations identified a phase with *I4/mcm* symmetry, one that remains the lowest-enthalpy structure in the whole pressure range studied. This polymorph is isostructural with a previously proposed high-pressure phase of Xe_2F [44]. Similarly to that structure, it contains an interpenetrating network of graphitic Kr layers (Figure 4a) with a Kr–Kr bond of about 2.5 Å at 150 GPa, which is ca 8% shorter than the Kr–Kr separation in solid krypton at the same pressure (Table 1). The second-nearest Kr–Kr contacts in Kr_2F are much longer (2.83–2.84 Å, Figure 4b), and the length of Kr–F contacts hints at no covalent bonding between krypton and fluorine (Table 1). In case of Xe_2F, Peng et al. indicated formation of covalent Xe–Xe bonds [44]. For Kr_2F we find, however, that ELF values between nearest-neighbor Kr atoms do not exceed 0.15 (Figure 4c), which hints at lack of Kr–Kr covalent bonding within the graphitic layers. Therefore, although the structure of Kr_2F features more directional contacts than Kr_6F and Kr_4F, it seems that it also can be described as built of relatively weekly bonded Kr and F atoms.

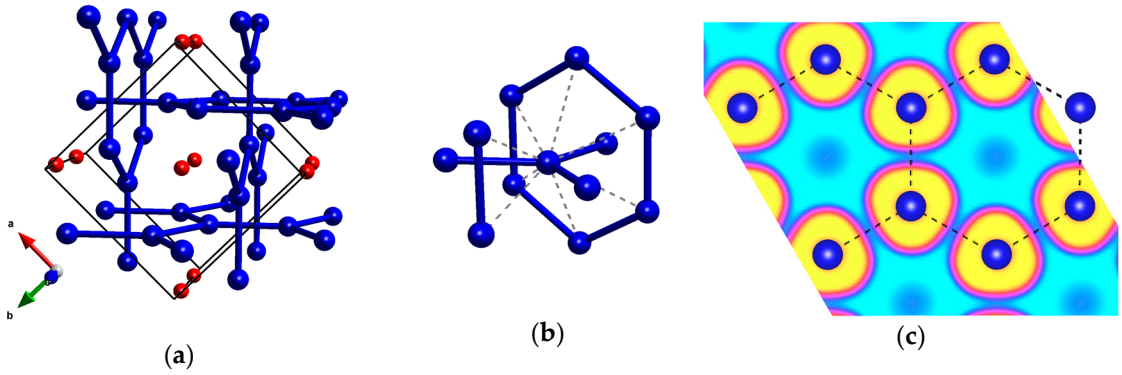

Figure 4. (**a**) the *I4/mcm* structure of Kr_2F; (**b**) the coordination environment of Kr with secondary Kr–Kr contacts marked with dashed lines; (**c**) ELF function for Kr_2F at 150 GPa. Yellow color depicts ELF values above 0.9, cyan—below 0.1, while magenta corresponds to values of 0.4. Shortest Kr–Kr contacts are marked with dashed lines.

Similarly to Kr_2F, we find that KrF exhibits only one polymorphic form in the whole pressure range studied. This structure of *P2/m* symmetry contains chains of Kr atoms (Figure 5a) with an extremely short Kr–Kr bond of 2.29 Å at 150 GPa (which is about 15% shorter than the Kr–Kr contact in solid krypton; see Table 1). At the same time, Kr–F and F–F shortest distances are considerably longer than those found in KrF_2 and F_2, respectively, while secondary Kr–Kr contacts are slightly longer to those found in solid Kr (Table 1, Figure 5b). These structural features indicate formation of Kr–Kr covalent bonds within the Kr chains. Indeed, inspection of the ELF function shows that the maximum ELF value along the shortest Kr–Kr distance is 0.4, comparable to what is found for KrF_2 and KrF_4 (Figure 5c). We note that Peng et al. found XeF to be thermodynamically stable at 100 GPa and 140 K [44]. However, their lowest enthalpy structure contained Xe–Xe dimers, instead of Kr chains found by us for KrF.

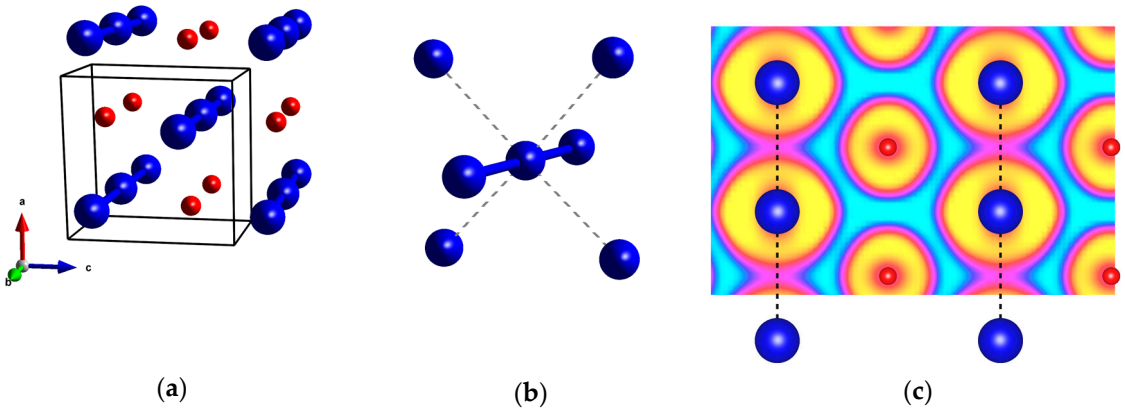

Figure 5. (**a**) the *P2/m* structure of KrF; (**b**) the coordination environment of Kr with secondary Kr–Kr contacts marked with dashed lines; (**c**) ELF function for KrF at 150 GPa. Yellow color depicts ELF values above 0.9, cyan—below 0.1, while magenta corresponds to values of 0.4. Shortest Kr–Kr contacts are marked with dashed lines.

3. Discussion

Previous theoretical studies on the reactivity of Xe/F [44] and Ar/F [30] systems indicated that application of high pressure leads to stabilization of compounds with high fluorine content (XeF_2, XeF_4, XeF_6, ArF_2) with respect to pure elements. We have found the same trend for the Kr/F system studied here—in particular we find that large compression should lead to thermodynamic stabilization of

a crystal containing KrF_4 molecules. If obtained, this compound would constitute the first example of a chemical connection containing krypton in the +4 oxidation state.

The increased reactivity of krypton compared to argon is evident from this study. We find that the stabilization pressure of KrF_4 is 15 GPa (more adequately approx. 40 GPa after taking into account overbinding due to the employed functional), while a compound containing ArF_4 molecules is predicted to form only above 250 GPa [30]—see Table 2. On the other hand, krypton remains less reactive than xenon at high pressure—our results indicate that KrF_6 is not stable at least up to 200 GPa, while XeF_6 can be obtained at ambient conditions.

Table 2. Comparison of the theoretical thermodynamic stability NgF_2, NgF_4, and NgF_6 (Ng = Ar, Kr, Xe) compounds up to pressures of 200 GPa. Pressures at which a given stoichiometry is stable are given in GPa (amb.—stable at ambient pressure; n.d.—not determined). For NgF_2 the numbers in parenthesis correspond to the decomposition pressure given in GPa.

Ng	NgF_2	NgF_4	NgF_6	Ref.
Ar	58 (> 200)	> 200	n.d.	[30]
Kr	amb. (180)	15	> 200	this work
Xe	amb. (81)	amb.	amb.	[44]

Pressures exceeding 50 GPa should lead to stabilization of krypton-rich fluorides (Kr_6F and Kr_4F at 80 GPa, Kr_2F at 140 GPa). This is in analogy with previous results for the Xe/F system, where stabilization of Xe_2F was predicted to occur above 60 GPa [44] (we note that in that study Xe_6F and Xe_4F compositions were not taken into account). We do not observe formation of direct bonds between noble-gas atoms in Kr_mF (m = 2, 4, 6) compounds, in contrast to Xe_2F, which does exhibit Xe–Xe bonds. We do however find Kr–Kr bond for KrF, which becomes stable at 100 GPa.

The enhanced thermodynamic stability of KrF at large compression influences the stability of KrF_2, which is predicted to decompose into KrF and KrF_4 at 180 GPa. Still, KrF_2 is more stable at large compression than XeF_2, which in turn is predicted to disproportionate into Xe_2F and XeF_4 above 81 GPa. Generally, it seems that the thermodynamic stability of noble-gas difluorides at high pressure increases, when moving up group 18 with ArF_2 predicted to dominate the convex hull of the Ar/F system up to 200 GPa [30].

We find that F–Kr–F molecules in KrF_2 undergo slight bending in response to compression, in analogy to ArF_2, but we do not encounter any signs of auto-ionization, as predicted for XeF_2 [42]. Interestingly, our structure searches do not identify any phases containing KrF^+ and $Kr_2F_3{}^+$ cations, which are known to form upon reaction of KrF_2 with fluoride acceptors [7]. This might hint at the fact that the fluoride-donor properties of KrF_2 are suppressed at large compression. In general, it seems that in the case of the Kr/F system, ionic bonding is not a major driving force in stabilization of high-pressure phases, in contrast to what is found for the N/F system [57].

We hope that the insight into the high-pressure chemistry of krypton offered by this study will motivate future investigation, in particular, experimental attempts to obtain KrF_4 and KrF. As already noted, the pressures necessary for the synthesis reported here are expected to be underestimated by about 25 GPa; nonetheless, even with this correction they fall well within the experimentally accessible pressure range achievable even with the use of commercially available diamond anvil cells. Most importantly, we note that both compounds should be accessible by a convenient pathway involving the high-pressure decomposition of KrF_2; such synthesis scheme should be preferred over the direct synthesis from Kr and F_2, in particular due to the large reactivity and toxicity of fluorine.

Finally, we note that a detailed study of the electronic properties of the Kr_mF_n compounds reported here would also be of interest. Analyzing the bands structure of these connections is beyond the scope of this study, we only note that our calculations indicate that Kr, F_2, KrF_2 and KrF_4 are semiconductors at 150 GPa, while Kr_6F, Kr_4F, Kr_2F and KrF are metallic at the same pressure (see Table S3 in SM).

4. Materials and Methods

Our study is based on periodic DFT calculations which were performed with the VASP 5.2 program [58–60]. We utilized the generalized gradient approximation (GGA) in the form of the Perdew–Burke–Ernzerhof (PBE) functional [61], which was successfully applied in previous high-pressure studies on xenon fluorides [42,44], as well as a recent study on the ambient-pressure structures of KrF_2 [62]. The projector augmented-wave (PAW) method was used [63], as implemented in the VASP 5.2 code. Our calculations do not included van der Waals corrections the DFT functional. We have found, however, that inclusion of such dispersion corrections (in the form of the D3 correction [64]) lead to negligible differences in the high-pressure thermodynamic stability of KrF_2 and KrF_4 (see Figures S1 and S2 in SM), in accordance with previous results for the Ar/F system [30].

The cut-off energy of the plane waves was set to 600 eV with a self-consistent-field convergence criterion of 1×10^{-5} eV. Valence electrons (Kr: 4s, 4p; F: 2s, 2p) were treated explicitly, while VASP pseudopotentials, accounting for scalar relativistic effects, were used for the description of core and semi-core electrons. The spacing of the *k*-point mesh was set at $2\pi \times 0.06$ Å^{-1}. All structures were optimized in 10 GPa steps (5 GPa below 20 GPa) using a conjugate gradient algorithm. Structure visualization was performed with the VESTA software [65], while symmetry recognition with the online FINDSYM program [66].

For each pressure, we optimize the structure of the studied Kr_mF_n phases, as well as that of elemental Kr and F_2. From the resulting enthalpies we derive the enthalpies of formation of Kr_mF_n phases at each pressure. At ambient pressure, krypton adopts the face-centered cubic (fcc) structure [67]. In our calculations, already at slightly elevated pressure (approx. 10 GPa) krypton adopts a hexagonal close-packed (hcp) structure and maintains it in the whole considered pressure range (0–200 GPa) We also note that, above 50 GPa, the ambient pressure structure of F_2 (*C2/c* space group [68]) symmetrizes spontaneously to a *Cmca* structure which is analogous to the high-pressure molecular polymorph of Cl_2 [69]. For a comparison of the experimental and calculated crystal structures of α-F2 and Kr at ambient pressure see Table S4 in the SM.

The candidate structures of Kr_mF_n were identified using the USPEX evolutionary algorithm [50,51] coupled with the PBE functional. The evolutionary searches were performed at P = 100 and 200 GPa with 1, 2 and 4 formula units per cell.

Supplementary Materials: The following are available online at http://www.mdpi.com/2073-4352/7/11/329/s1, Table S1: Structure parameters of the most stable polymorphs of Kr_3F_2, KrF_2 and KrF_4, Table S2: Structure parameters of the most stable polymorphs of K_6F, Kr_4F, Kr_2F and KrF, Table S3: Calculated band gaps for the lowest enthalpy structures of Kr_mF_n compounds at 150 GPa, Table S4: Comparison of the experimental and calculated (PBE method) crystal structures of α-F_2 and Kr at ambient pressure, Figure S1: Comparison of the relative enthalpy of the ambient pressure *P42/mnm* structure of KrF_2 with respect to the high-pressure *Cmcm* structure obtained with three different computational methods (PBE, PBE+D3, HSE06), Figure S2: Comparison of the enthalpy change of the reaction $KrF_2 + F_2$ -> KrF_3 obtained with three different computational methods (PBE, PBE+D3, HSE06). The ambient pressure CCSD(T) value calculated with the use of data from Dixon et al. (ref. [55]) is marked with a star. Figure S3: (**a**) The *P–1* structure of Kr_6F obtained at 150 GPa; (**b**) the *C2/m* structure of Kr_4F at 150 GPa, Figure S4: The ELF function at 150 GPa for: (**a**) the *P–1* structure of Kr_6F; (**b**) the *C2/m* structure of Kr_4F; (**c**) the hcp structure of Kr.

Acknowledgments: Dominik Kurzydłowski acknowledges the support from the Polish National Science Centre (NCN) within grant No. UMO-2014/13/D/ST5/02764. This research was carried out with the support of the Interdisciplinary Centre for Mathematical and Computational Modelling (ICM) University of Warsaw under grant No. GA67–13.

Author Contributions: Dominik Kurzydłowski and Patryk Zaleski-Ejgierd conceived and designed the research; Magdalena Sołtysiak and Aleksandra Dżoleva performed the calculations; Dominik Kurzydłowski, Magdalena Sołtysiak, Aleksandra Dżoleva and Patryk Zaleski-Ejgierd analyzed the data; Dominik Kurzydłowski wrote the paper.

Conflicts of Interest: The authors declare no conflict of interest. The founding sponsors had no role in the design of the study; in the collection, analyses, or interpretation of data; in the writing of the manuscript, and in the decision to publish the results.

References

1. Tramšek, M.; Žemva, B. Synthesis, properties and chemistry of xenon(II) fluoride. *Acta Chim. Slov.* **2006**, 105–116. [CrossRef]
2. Grochala, W. Atypical compounds of gases, which have been called "noble". *Chem. Soc. Rev.* **2007**, *36*, 1632–1655. [CrossRef] [PubMed]
3. Nabiev, S.S.; Sokolov, V.B.; Chaivanov, B.B. Structure of simple and complex noble gas fluorides. *Crystallogr. Rep.* **2011**, *56*, 774–791. [CrossRef]
4. Brock, D.S.; Schrobilgen, G.J.; Žemva, B. Noble-Gas Chemistry. In *Comprehensive Inorganic Chemistry II*; Elsevier: Cambridge, MA, USA, 2013; pp. 755–822.
5. Nabiev, S.S.; Sokolov, V.B.; Chaivanov, B.B. Molecular and crystal structures of noble gas compounds. *Russ. Chem. Rev.* **2014**, *83*, 1135–1180. [CrossRef]
6. Haner, J.; Schrobilgen, G.J. The chemistry of Xenon(IV). *Chem. Rev.* **2015**, *115*, 1255–1295. [CrossRef] [PubMed]
7. Lehmann, J.F.; Mercier, H.P.A.; Schrobilgen, G.J. The chemistry of krypton. *Coord. Chem. Rev.* **2002**, *233–234*, 1–39. [CrossRef]
8. Lozinšek, M.; Schrobilgen, G.J. The world of krypton revisited. *Nat. Chem.* **2016**, *8*, 732. [CrossRef] [PubMed]
9. Lozinšek, M.; Mercier, H.P.A.; Brock, D.S.; Žemva, B.; Schrobilgen, G.J. Coordination of KrF_2 to a Naked Metal Cation, Mg^{2+}. *Angew. Chem. Int. Ed.* **2017**, *56*, 6251–6254. [CrossRef] [PubMed]
10. Grosse, A.V.; Kirshenbaum, A.D.; Streng, A.G.; Streng, L.V. Krypton Tetrafluoride: Preparation and Some Properties. *Science* **1963**, *139*, 1047–1048. [CrossRef] [PubMed]
11. Brown, T.H.; Verdier, P.H. Krypton Tetrafluoride: 19F High-Resolution Magnetic Resonance Spectrum. *J. Chem. Phys.* **1964**, *40*, 2057. [CrossRef]
12. Turner, J.J.; Pimentel, G.C. Krypton Fluoride: Preparation by the Matrix Isolation Technique. *Science* **1963**, *140*, 974–975. [CrossRef] [PubMed]
13. Schreiner, F.; Malm, J.G.; Hindman, J.C. The Preparation and Nuclear Magnetic Resonance of Krypton Difluoride. *J. Am. Chem. Soc.* **1965**, *87*, 25–28. [CrossRef]
14. Bartlett, N. Xenon hexafluoroplatinate(V) $Xe^{+}[PtF6]^{-}$. *Proc. Chem. Soc.* **1962**, *6*, 218.
15. Hargittai, I. Neil Bartlett and the first noble-gas compound. *Struct. Chem.* **2009**, *20*, 953–959. [CrossRef]
16. Gunn, S.R. Heat of formation of krypton difluoride. *J. Phys. Chem.* **1967**, *71*, 2934–2937. [CrossRef]
17. Chen, J.L.; Yang, C.Y.; Lin, H.J.; Hu, W.P. Theoretical prediction of new noble-gas molecules FNgBNR (Ng = Ar, Kr, and Xe; R = H, CH3, CCH, CHCH2, F, and OH). *Phys. Chem. Chem. Phys.* **2013**, *15*, 9701. [CrossRef] [PubMed]
18. Gronowski, M.; Turowski, M.; Kołos, R. Quantum Chemical Study on $HKrC_5N$, $HXeC_5N$, and Related Rare Gas Compounds. *J. Phys. Chem. A* **2015**, *119*, 2672–2682. [CrossRef] [PubMed]
19. Ghosh, A.; Manna, D.; Ghanty, T.K. Theoretical Prediction of Noble Gas Inserted Thioformyl Cations: $HNgCS^{+}$ (Ng = He, Ne, Ar, Kr, and Xe). *J. Phys. Chem. A* **2015**, *119*, 2233–2243. [CrossRef] [PubMed]
20. Joseph, J.A.; McDowell, S.A.C. Comparative computational study of model halogen-bonded complexes of FKrCl. *J. Phys. Chem. A* **2015**, *119*, 2568–2577. [CrossRef] [PubMed]
21. Zhang, Q.; Chen, M.; Zhou, M.; Andrada, D.M.; Frenking, G. Experimental and theoretical studies of the infrared spectra and bonding properties of $NgBeCO_3$ and a comparison with NgBeO (Ng = He, Ne, Ar, Kr, Xe). *J. Phys. Chem. A* **2015**, *119*, 2543–2552. [CrossRef] [PubMed]
22. Saha, R.; Pan, S.; Mandal, S.; Orozco, M.; Merino, G.; Chattaraj, P.K. Noble gas supported B_3^{+} cluster: Formation of strong covalent noble gas–boron bonds. *RSC Adv.* **2016**, *6*, 78611–78620. [CrossRef]
23. Chen, W.; Chen, G.H.; Wu, D.; Wang, Q. BNg_3F_3: The first three noble gas atoms inserted into mono-centric neutral compounds—A theoretical study. *Phys. Chem. Chem. Phys.* **2016**, *18*, 17534–17545. [CrossRef] [PubMed]
24. Khriachtchev, L.; Pettersson, M.; Runeberg, N.; Lundell, J.; Räsänen, M. A stable argon compound. *Nature* **2000**, *406*, 874–876. [PubMed]
25. Evans, C.J.; Gerry, M.C.L. The microwave spectra and structures of Ar–AgX (X = F, Cl, Br). *J. Chem. Phys.* **2000**, *112*, 1321–1329. [CrossRef]
26. Grochala, W.; Khriachtchev, L.; Räsänen, M. Noble-gas chemistry. In *Physics & Chemistry at Low Temperatures*; Khriachtchev, L., Ed.; Pan Stanford Publishing: Boca Raton, FL, USA, 2011; pp. 419–446.

27. Grandinetti, F. Review: Gas-phase ion chemistry of the noble gases: Recent advances and future perspectives. *Eur. J. Mass Spectrom.* **2011**, *17*, 423–463. [CrossRef] [PubMed]
28. Young, N.A. Main group coordination chemistry at low temperatures: A review of matrix isolated Group 12 to Group 18 complexes. *Coord. Chem. Rev.* **2013**, *257*, 956–1010. [CrossRef]
29. Wang, X.; Andrews, L.; Brosi, F.; Riedel, S. Matrix Infrared Spectroscopy and Quantum-Chemical Calculations for the Coinage-Metal Fluorides: Comparisons of Ar-AuF, Ne-AuF, and Molecules MF_2 and MF_3. *Chem. A Eur. J.* **2013**, *19*, 1397–1409. [CrossRef] [PubMed]
30. Kurzydłowski, D.; Zaleski-Ejgierd, P. High-pressure stabilization of argon fluorides. *Phys. Chem. Chem. Phys.* **2016**, *18*, 2309–2313. [CrossRef] [PubMed]
31. Somayazulu, M.; Dera, P.; Smith, J.; Hemley, R.J. Structure and stability of solid $Xe(H_2)_n$. *J. Chem. Phys.* **2015**, *142*, 104503. [CrossRef] [PubMed]
32. Dewaele, A.; Worth, N.; Pickard, C.J.; Needs, R.J.; Pascarelli, S.; Mathon, O.; Mezouar, M.; Irifune, T. Synthesis and stability of xenon oxides Xe_2O_5 and Xe_3O_2 under pressure. *Nat. Chem.* **2016**, *8*, 784–790. [CrossRef] [PubMed]
33. Howie, R.T.; Turnbull, R.; Binns, J.; Frost, M.; Dalladay-Simpson, P.; Gregoryanz, E. Formation of Xenon-nitrogen compounds at high pressure. *Sci. Rep.* **2016**, *6*, 34896. [CrossRef] [PubMed]
34. Dewaele, A.; Pépin, C.M.; Geneste, G.; Garbarino, G. Reaction between nickel or iron and xenon under high pressure. *High Press. Res.* **2017**, *37*, 137–146. [CrossRef]
35. Dong, X.; Oganov, A.R.; Goncharov, A.F.; Stavrou, E.; Lobanov, S.; Saleh, G.; Qian, G.R.; Zhu, Q.; Gatti, C.; Deringer, V.L.; et al. A stable compound of helium and sodium at high pressure. *Nat. Chem.* **2017**, *9*, 440–445. [CrossRef] [PubMed]
36. Zhu, Q.; Jung, D.Y.; Oganov, A.R.; Glass, C.W.; Gatti, C.; Lyakhov, A.O. Stability of xenon oxides at high pressures. *Nat. Chem.* **2013**, *5*, 61–65. [CrossRef] [PubMed]
37. Hermann, A.; Schwerdtfeger, P. Xenon Suboxides Stable under Pressure. *J. Phys. Chem. Lett.* **2014**, *5*, 4336–4342. [CrossRef] [PubMed]
38. Yan, X.; Chen, Y.; Xiang, S.; Kuang, X.; Bi, Y.; Chen, H. High-temperature- and high-pressure-induced formation of the Laves-phase compound XeS_2. *Phys. Rev. B* **2016**, *93*, 214112. [CrossRef]
39. Zaleski-Ejgierd, P.; Lata, P.M. Krypton oxides under pressure. *Sci. Rep.* **2016**, *6*, 18938. [CrossRef] [PubMed]
40. Hou, C.; Wang, X.; Botana, J.; Miao, M. Noble gas bond and the behaviour of XeO_3 under pressure. *Phys. Chem. Chem. Phys.* **2017**, *19*, 27463–27467. [CrossRef] [PubMed]
41. Kim, M.; Debessai, M.; Yoo, C.S. Two- and three-dimensional extended solids and metallization of compressed XeF_2. *Nat. Chem.* **2010**, *2*, 784–788. [CrossRef] [PubMed]
42. Kurzydłowski, D.; Zaleski-Ejgierd, P.; Grochala, W.; Hoffmann, R. Freezing in resonance structures for better packing: XeF_2 becomes $(XeF^+)(F^-)$ at large compression. *Inorg. Chem.* **2011**, *50*, 3832–3840. [CrossRef] [PubMed]
43. Wu, G.; Huang, X.; Huang, Y.; Pan, L.; Li, F.; Li, X.; Liu, M.; Liu, B.; Cui, T. Confirmation of the Structural Phase Transitions in XeF_2 under High Pressure. *J. Phys. Chem. C* **2017**, *121*, 6264–6271. [CrossRef]
44. Peng, F.; Botana, J.; Wang, Y.; Ma, Y.; Miao, M. Unexpected trend in stability of Xe–F compounds under pressure driven by Xe–Xe covalent bonds. *J. Phys. Chem. Lett.* **2016**, 4562–4567. [CrossRef] [PubMed]
45. Braïda, B.; Hiberty, P.C. The essential role of charge-shift bonding in hypervalent prototype XeF_2. *Nat. Chem.* **2013**, *5*, 417–422. [CrossRef] [PubMed]
46. Oganov, A.R.; Lyakhov, A.O.; Valle, M. How evolutionary crystal structure prediction works—And why. *Acc. Chem. Res.* **2011**, *44*, 227–237. [CrossRef] [PubMed]
47. Zurek, E.; Grochala, W. Predicting crystal structures and properties of matter under extreme conditions via quantum mechanics: The pressure is on. *Phys. Chem. Chem. Phys.* **2015**, *17*, 2917–2934. [CrossRef] [PubMed]
48. Needs, R.J.; Pickard, C.J. Perspective: Role of structure prediction in materials discovery and design. *APL Mater.* **2016**, *4*, 53210. [CrossRef]
49. Zhang, L.; Wang, Y.; Lv, J.; Ma, Y. Materials discovery at high pressures. *Nat. Rev. Mater.* **2017**, *2*, 17005. [CrossRef]
50. Glass, C.W.; Oganov, A.R.; Hansen, N. USPEX—Evolutionary crystal structure prediction. *Comput. Phys. Commun.* **2006**, *175*, 713–720. [CrossRef]
51. Oganov, A.R.; Glass, C.W. Crystal structure prediction using ab initio evolutionary techniques: Principles and applications. *J. Chem. Phys.* **2006**, *124*, 244704. [CrossRef] [PubMed]

52. Feng, J.; Hennig, R.G.; Ashcroft, N.W.; Hoffmann, R. Emergent reduction of electronic state dimensionality in dense ordered Li-Be alloys. *Nature* **2008**, *451*, 445–448. [CrossRef] [PubMed]
53. Lehmann, J.F.; Dixon, D.A.; Schrobilgen, G.J. X-ray crystal structures of α-KrF_2, [KrF][MF_6] (M = As, Sb, Bi), [Kr_2F_3][SbF_6]·KrF_2, [Kr_2F_3]$_2$[SbF_6]$_2$·KrF_2, and [Kr_2F_3][AsF_6]·[KrF][AsF_6]; synthesis and characterization of [Kr_2F_3][PF_6]·nKrF_2; and theoretical studies of KrF_2, KrF^+, Kr_2F^{3+}, and the [KrF][MF_6] (M = P, As, Sb, Bi) ion pairs. *Inorg. Chem.* **2001**, *40*, 3002–3017. [PubMed]
54. Burbank, R.D.; Falconer, W.E.; Sunder, W.A. Crystal Structure of Krypton Difluoride at −80 °C. *Science* **1972**, *178*, 1285–1286. [CrossRef] [PubMed]
55. Dixon, D.A.; Wang, T.H.; Grant, D.J.; Peterson, K.A.; Christe, K.O.; Schrobilgen, G.J. Heats of formation of krypton fluorides and stability predictions for KrF_4 and KrF_6 from high level electronic structure calculations. *Inorg. Chem.* **2007**, *46*, 10016–10021. [CrossRef] [PubMed]
56. Savin, A.; Nesper, R.; Wengert, S.; Fässler, T.F. ELF: The electron localization function. *Angew. Chem. Int. Ed. Engl.* **1997**, *36*, 1808–1832. [CrossRef]
57. Kurzydłowski, D.; Zaleski-Ejgierd, P. Hexacoordinated nitrogen(V) stabilized by high pressure. *Sci. Rep.* **2016**, *6*, 36049. [CrossRef] [PubMed]
58. Kresse, G.; Furthmüller, J. Efficiency of ab-initio total energy calculations for metals and semiconductors using a plane-wave basis set. *Comput. Mater. Sci.* **1996**, *6*, 15–50. [CrossRef]
59. Kresse, G.; Furthmüller, J. Efficient iterative schemes for ab initio total-energy calculations using a plane-wave basis set. *Phys. Rev. B* **1996**, *54*, 11169–11186. [CrossRef]
60. Kresse, G.; Joubert, D. From ultrasoft pseudopotentials to the projector augmented-wave method. *Phys. Rev. B* **1999**, *59*, 1758–1775. [CrossRef]
61. Perdew, J.P.; Burke, K.; Ernzerhof, M. Generalized Gradient Approximation Made Simple. *Phys. Rev. Lett.* **1996**, *77*, 3865–3868. [CrossRef] [PubMed]
62. Galy, J.; Matar, S.F. ns^2np^4 (n = 4, 5) lone pair triplets whirling in M*F_2E_3 (M* = Kr, Xe): Stereochemistry and ab initio analyses. *Solid State Sci.* **2017**, *64*, 114–124. [CrossRef]
63. Blöchl, P.E. Projector augmented-wave method. *Phys. Rev. B* **1994**, *50*, 17953–17979. [CrossRef]
64. Grimme, S.; Antony, J.; Ehrlich, S.; Krieg, H. A consistent and accurate ab initio parametrization of density functional dispersion correction (DFT-D) for the 94 elements H-Pu. *J. Chem. Phys.* **2010**, *132*, 154104. [CrossRef] [PubMed]
65. Momma, K.; Izumi, F. VESTA: A three-dimensional visualization system for electronic and structural analysis. *J. Appl. Crystallogr.* **2008**, *41*, 653–658. [CrossRef]
66. Stokes, H.T.; Hatch, D.M. FINDSYM: Program for identifying the space-group symmetry of a crystal. *J. Appl. Crystallogr.* **2005**, *38*, 237–238. [CrossRef]
67. Figgins, B.F.; Smith, B.L. Density and expansivity of solid krypton. *Philos. Mag.* **1960**, *5*, 186–188. [CrossRef]
68. Pauling, L.; Keaveny, I.; Robinson, A.B. The crystal structure of α-fluorine. *J. Solid State Chem.* **1970**, *2*, 225–227. [CrossRef]
69. Johannsen, P.G.; Holzapfel, W.B. Effect of pressure on Raman spectra of solid chlorine. *J. Phys. C Solid State Phys.* **1983**, *16*, L1177–L1179. [CrossRef]